Electronic Supplementary Material (ESI) for ChemComm.

Multi-Principal Element Transition Metal Dichalcogenides via Reactive Fusion of 3D-Heterostructures

Ihor Z. Hlova,[a] Oleksandr Dolotko,[a] Brett W. Boote,[ab] Arjun K. Pathak,[a] Emily A. Smith,[ab] Vitalij K. Pecharsky,[a,c] Viktor P. Balema[a]*

[a] Ames Laboratory of U.S. Department of Energy, Iowa State University, Ames, IA, 50011-2416, E-mail: vbalema@ameslab.gov

[b] Department of Chemistry, Iowa State University, Ames, IA, 50011-1021

[c] Department of Materials Science and Engineering, Iowa State University, Ames, IA, 50011-1096

Supporting Information

Experimental details

Materials: Ultra-high purity Ar (Matheson, 99.999%), ultra-high purity He (Matheson, 99.999%), MoS_2 (Sigma-Alrdich, 99% purity), WS_2 (Sigma-Alrdich, 99% purity), $MoSe_2$ (Alfa Aesar, 99.9% purity), WSe_2 (Alfa Aesar, 99.8% purity), $NbSe_2$ (Alfa Aesar, 99.8% purity). TaS_2 was prepared in-house from Ta powder (99.99% purity) and S (Alfa Aesar, 99.9995% purity). Commercially available transition metal dichalcogenides (TMDCs), MoS_2, WS_2, $MoSe_2$, WSe_2 and $NbSe_2$, were used as starting materials without further purification.

Preparation of multi-principal element TMDCs: In a typical experiment, a 2 g sample of a physical mixture of two or more different binary TMDCs, taken in an appropriate stoichiometric proportion, was milled in either stainless steel milling container with eight 11.9 mm stainless steel balls, or in a silicon nitride vial with three 12.7 mm silicon nitride grinding balls using a two-station horizontal planetary mill (Fritsch, Pulverisette 7), or a shaker mill (SPEX 8000M) for various periods of time (1–30 hours). The milling containers were loaded and sealed under ultra-high purity argon in a glove box. To facilitate uniform milling and to prevent kinking of the powder during the processing, the milling mode of the planetary mill was alternated between forward and reverse rotations (30 min each) with an intermittent pause of 5 min. Subsequently, as-milled powders were pressed into pellets under argon in a glove box, placed in a quartz tube, which was further sealed under 0.75 bar of ultra-high purity helium. Typically, the heat treatment was conducted by ramping the temperature to 1000 °C and annealing the material for 16 hours or longer. Afterwards, samples were allowed to cool down to room temperature in the furnace. For analytical characterization, prepared materials were crushed in a mortar with a pestle and stored in a glove box under high-purity argon.

The material of the milling equipment does not affect the overall outcome of the synthetic process. Also, according to X-ray fluorescence spectrometry (XRF), samples prepared using the hardened steel setup contained up to 0.4 at.% of iron contamination.

Exfoliation of $(Mo_{0.5}W_{0.5})SSe$: The exfoliation of the single-phase heat-treated $(Mo_{0.5}W_{0.5})SSe$ was conducted using the ultrasonic homogenizer (Q 700, Qsonica) equipped with a ¾ inch diameter probe. During the experiment, 0.5 g of material was added to 100 ml of iso-propanol and sonicated at 50 % amplitude for 5 hours. The temperature of solution was kept in the range of 15-25 °C by external ice-cooling. Thereafter, the obtained suspension was centrifuged at 3500 rpm for 15 min, the liquid phase was separated and used for further analysis.

Powder X-ray Diffraction (XRD): The measurements were carried out using a PANalytical X'PERT powder diffractometer with an Xcelerator detector in the 2θ range from 10° to 80° with 0.02° step size employing Cu-Kα1 radiation (λ = 0.15406 nm).

Thermogravimetric Analysis (TGA): TGA data were collected using Netzsch Luxx STA 409 PG. About 10 mg of the investigated materials were placed in alumina crucibles and heated up under argon from room temperature to 1450 °C with a ramping rate of 10 °C/min.

HAADF-STEM and STEM-EDS measurements: TEM experiments were performed on a Titan Themis (FEI) probe Cs-corrected TEM. High-resolution HAADF-STEM images were collected by the convergence semi-angle of 18 mrad and a collection semi-angle of 99-200 mrad at 200 kV. STEM-EDS analysis was carried out using a Super-X EDS detector attached to the Titan Themis. Focused Ion Beam (FIB) cross-sectioning was performed on a Helios Nanolab G3 UC dual-beam instrument (FEI). A liftout for TEM was carried out using standard in-situ TEM liftout procedures[1] by means of the EZLift micromanipulator and Multi-Chem gas injection system. For the FIB cross-sectioning, a large agglomerate of particles was selected and covered with a protective layer of carbon that prevented the sputtering of the top surface of the sample during the experiment. Next, a trench was sputtered from both sides of the particle, resulting in a rectangular shape specimen, which afterwards was attached to a tungsten needle and thinned to electron transparency.

STEM-EDS results observed for the *as-milled* MoS_2-WS_2 and MoS_2-WSe_2 materials can be fully understood once the type of the information provided by each of these analytical techniques is considered. While XRD and Raman spectroscopy are probing structural features and chemical bonding in the investigated solids, EDS yields the chemical composition of a sample averaged over the excitation volume within the penetration depth of the electron beam.[2] Even if the beam is sharply focused (<10 nm in the cross-section for STEM-EDS), its penetration depth varies between tens and hundreds of nanometers, depending on the beam's intensity and electron absorption by the elements constituting the material. These penetration depths clearly exceed the thickness of a single TMDC layer (~0.6 nm) and EDS-derived composition of a TMDC particle is averaged over a multi-layer volume. Hence, the material may appear compositionally uniform even though it is built from alternating, chemically dissimilar building blocks. It is also worth noting that because of interferences (Mo and S), STEM-EDS technique offers rather qualitative analytical value.

Raman Spectroscopy: Powdered samples were spread on glass cover slips and analysed with a Horiba XploRA Raman microscope (HORIBA Scientific, Edison, NJ) using 532-nm excitation ($8.3 \cdot 103$ W/cm^2) and a 100× (0.90 NA) objective. The detector was a front-illuminated Horiba Synapse EMCCD camera, and the acquisition time was 60 seconds. For each sample, the displayed spectrum was an average of 10 locations.

High-resolution X-ray photoelectron spectra (XPS): Measurements were carried out for compositional analysis. A few milligrams of powder samples were mounted on a double-sided Scotch tape. XPS spectra for S 2p, Se 3d, Mo 3d and W 4f were acquired using physical electronic 5500 multi technique system with an Al-Kα source. To compensate the charging effects, the binding energies of all peaks were corrected using standard carbon peak at 285 eV.

Preparation of TaS_2: TaS_2 was prepared by ball-milling and heat treatment of a nearly stoichiometric mixture of tantalum and sulfur (5% excess). The milling was performed for 4 hours, then it was followed by a 5-day heat treatment of the powder formed in a quartz tube sealed under 0.75 bar pressure of the ultra-high purity helium. The XRD analysis for the obtained material indicated the formation of the pure TaS_2 phase (Fig. SE1).

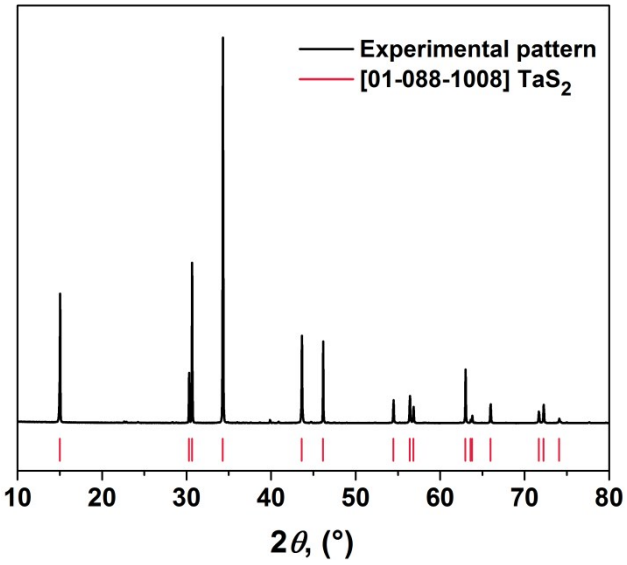

Fig. SE1 TaS_2 prepared from the elements. Vertical bars at the bottom of the chart correspond to Bragg peak positions of TaS_2.

Additional experimental details: It is worth noting that the frequency of milling has a distinct effect on its result. Thus, the XRD pattern of the materials processed for 30 hours in the planetary mill at 300 rpm (processing frequency of 5 Hz) is quite similar to that obtained after one hour of milling of the MoS_2 and WSe_2 mixture in a SPEX 8000M unit (processing frequency of ~ 18 Hz), and the XRD pattern of the sample processed for 4 hours in the SPEX 8000M mill closely resembles that of the powder generated in the Fritsch Pulverisette 7 planetary mill at 600 rpm (the processing frequency of 10Hz) for 30 hours (Fig. SE2).

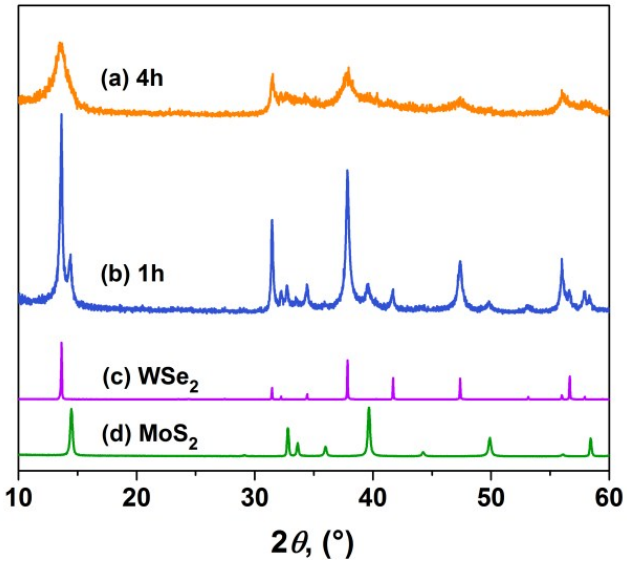

Fig. SE2 XRD of *as-milled* equimolar mixture of MoS_2 and WSe_2. The material was processed in a silicon nitride milling set using SPEX 8000M shaker mill for 4h (a) and 1h (b). XRD patterns of WSe_2 (c) and MoS_2 (d) are shown as reference.

The material of the milling equipment does not seem to affect the overall outcome of the synthetic process and a single-phase $(Mo_{0.5}W_{0.5})SSe$ could be successfully prepared in both silicon nitride and hardened steel vials after heat treatment. In the latter case, processed material contained up to 0.4 at.% of iron contamination after 30 hours of milling as determined by X-ray fluorescence spectrometry (XRF). Similar amount of iron was also discovered in other TMDC samples prepared using the hardened steel milling sets.

Rietveld refinement: The phase analysis and structural characterization of the reactions products was carried out by powder X-ray diffraction (XRD) analysis at room temperature on a PANalytical powder diffractometer using Cu-$K_{\alpha 1}$ radiation with a 0.02° 2θ step, in the range of Bragg angles 2θ from 10° to 80°. Rietveld refinements were performed using FullProf.[3] The background of all powder diffraction patterns was fitted using linear interpolations between selected data points from regions with no Bragg peaks present. The Thompson-Cox-Hastings pseudo-Voigt function was used for the peak profile shape description. The scale factor, lattice parameters, fractional coordinates of atoms and their isotropic displacement parameters, zero shift, profile shape parameters and half width (Caglioti) parameters were allowed to vary during the fitting. The least-square minimization had shown systematic divergence when the M/X (M = Mo, W, Nb, Ta and X = S or Se) occupations were treated as independent parameters. In order to improve the stability of calculations, the occupation factors of all components were restrained to the compositions of the starting mixtures. The instrumental resolution function was determined for NIST LaB_6 standard reference material and explicitly used for calculation of the reflections half widths. Additional peak broadening from the sample was taken into account as a phase-specific microstrain and crystalline size effect. Anisotropic broadening of (*h* 0 *l*) Bragg peaks due to the plate-like particle shapes is largely responsible for relatively high R_ps. As expected, increased milling time and energy leads to a continuing reduction of the average crystallite sizes (Table SE1).

Table S1. Average grain sizes as estimated from the XRD data during Rietveld refinements.

Sample description	Average grain size, Å	XRD pattern location
as-milled		
MoS_2 & WSe_2 (50:50 at.%) milled using a Si_3N_4 setup in SPEX 8000M for 1h	MoS_2 – 218 WSe_2 – 301	Fig. SE2b
MoS_2 & WSe_2 (50:50 at.%) milled using a Si_3N_4 setup in SPEX 8000M for 4h	MoS_2 – 91 WSe_2 – 68	Fig. SE2a
MoS_2 & WSe_2 (50:50 at.%) milled using steel setup in Fritsch Pulverisette 7 for 1h	MoS_2 – 517 WSe_2 – 1445	Fig. S7a
MoS_2 & WSe_2 (50:50 at.%) milled using steel setup in Fritsch Pulverisette 7 for 10h	MoS_2 – 303 WSe_2 – 824	Fig. S7b
MoS_2 & WSe_2 milled using steel setup in Fritsch Pulverisette 7 for 30h	MoS_2 – 221 WSe_2 – 350	Fig. S7c
fused		
$Mo_{0.5}W_{0.5}SSe$ after milling at 300 rpm and annealing at 1000 C for 16 h.	1923	Fig. S9a
$Mo_{0.5}W_{0.5}SSe$	1081	Fig. SE3
$Mo_{0.5}W_{0.5}S_2$	941	Fig. 1a
$Mo_{0.4}W_{0.2}Nb_{0.4}S_{0.8}Se_{1.2}$	534	Fig. S5a
$Mo_{0.6}W_{0.2}Ta_{0.2}S_{0.8}Se_{1.2}$	1938	Fig. S5c
$Mo_{0.25}W_{0.25}Nb_{0.25}Ta_{0.25}SSe$	585	Fig. S5e

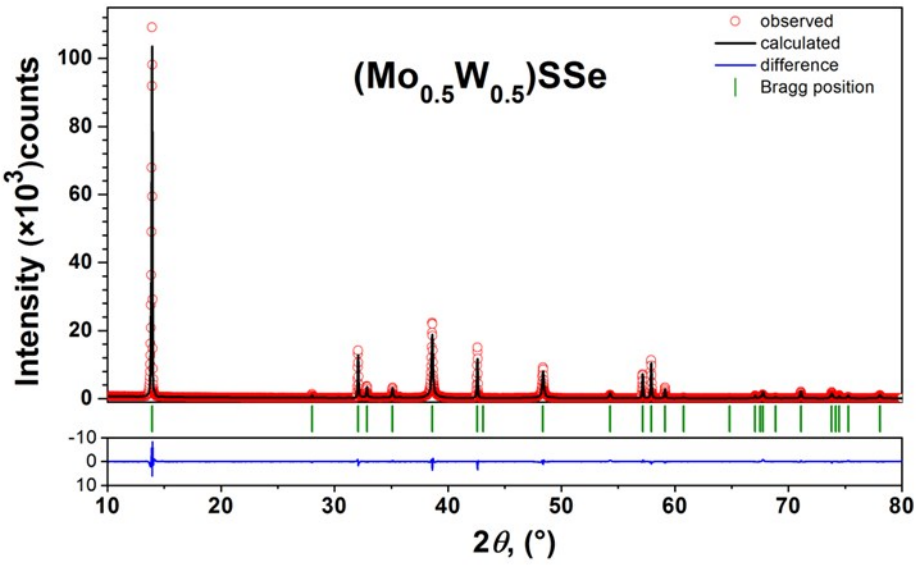

Fig. SE3 Example for the Rietveld refinement of the structure model based on XRD data of $(Mo_{0.5}W_{0.5})SSe$. Vertical bars at the bottom of the chart mark calculated positions of Bragg peaks of the refined phase. The material crystallizes in space group $P6_3/mmc$, common for layered TMDCs, where Mo and W atoms randomly occupy the 2c position (1/3, 2/3, 1/4) in the crystal lattice. The 4f site (1/3, 2/3, z) is filled randomly with S and Se. Shapes of Bragg reflections in the XRD pattern are highly anisotropic owing to distinctly plate-shaped particles and a nonrandom distribution of their orientations, which causes texturing and asymmetric broadening of the (*h* 0 *l*) Bragg peaks. Corrections for these effects require spherical harmonics expansion to approximate crystallite shapes[4] for Rietveld-based refinements,[3] results of which for this and other compounds described in this work are listed in Table 1.

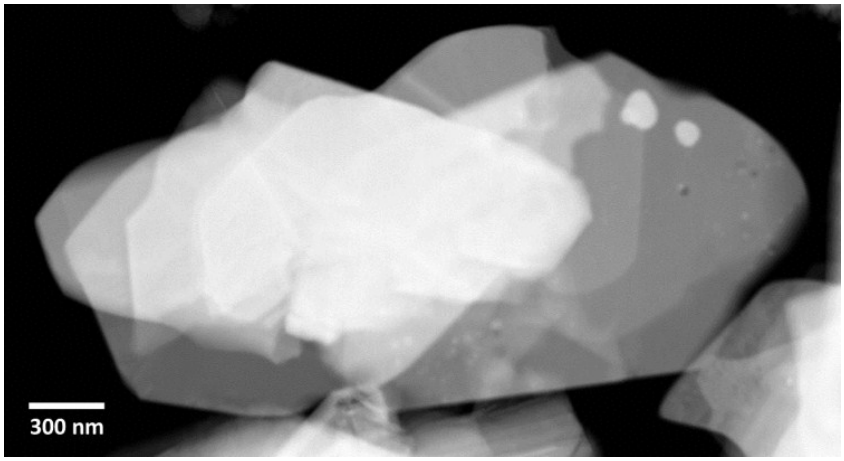

Fig. SE4 HAADF-STEM image of a typical particle of $(W_{0.5}Mo_{0.5})SSe$.

All experiments described in this work were repeated several times to ensure their reproducibility.

Figures referenced in the text

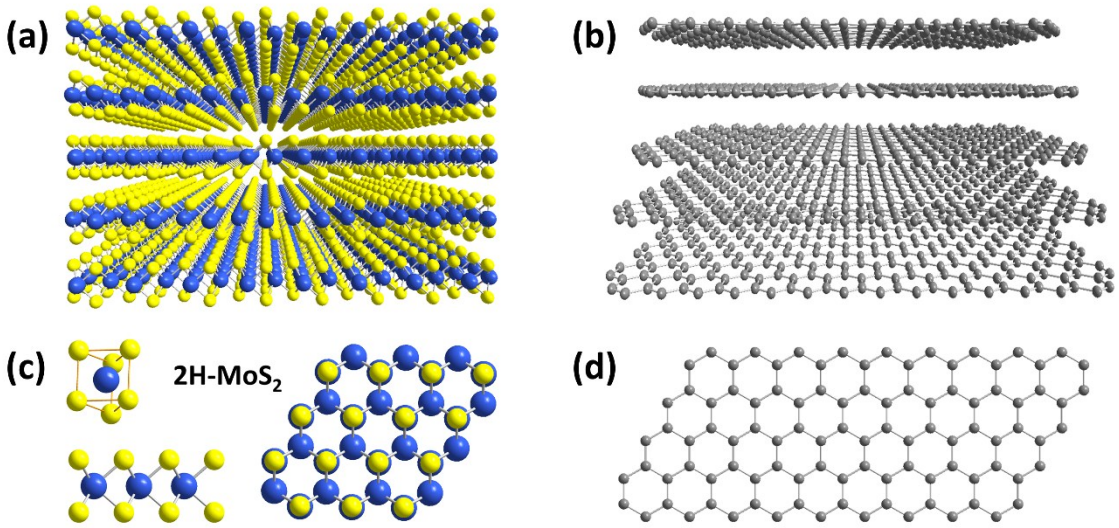

Fig. S1 Structure of layered van der Waals materials. (a) Transition metal dichalcogenides MX_2, where M is refractory metal such as Mo, W, Nb or Ta and X is S or Se. (b) Graphite. (c) The side and top-views of the 2H-modification of 2D-MX_2, and (d) the top-view of graphene.

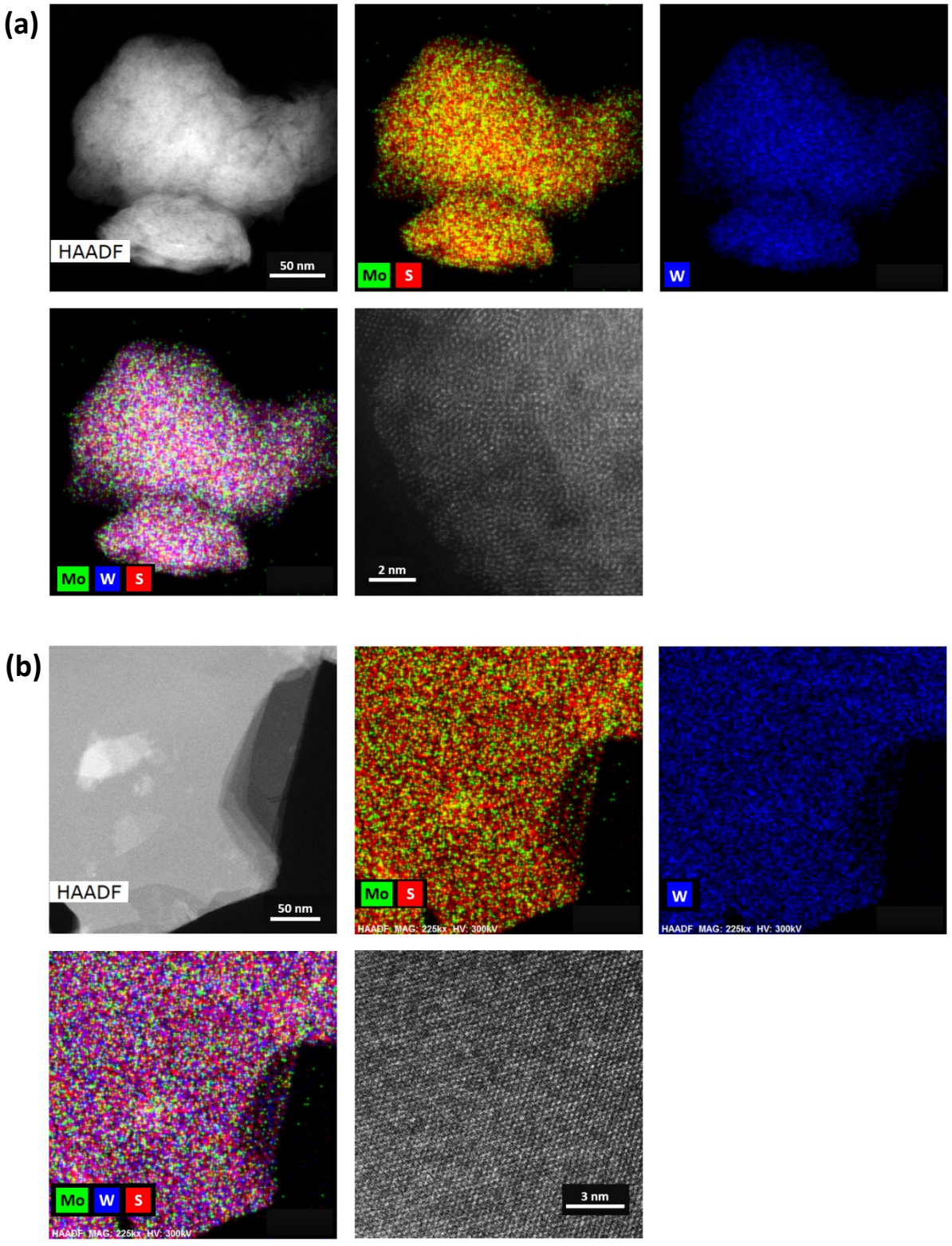

Fig. S2 $(Mo_{0.5}W_{0.5})S_2$. HAADF-STEM and STEM-EDS images of *as-milled* (a) and milled then fused materials (b). Intensity variations in the high-resolution HAADF-STEM images are due to different Z-factors of W (brighter spots) and Mo (darker spots). Due to X-ray signal overlap, Mo and S are shown together.

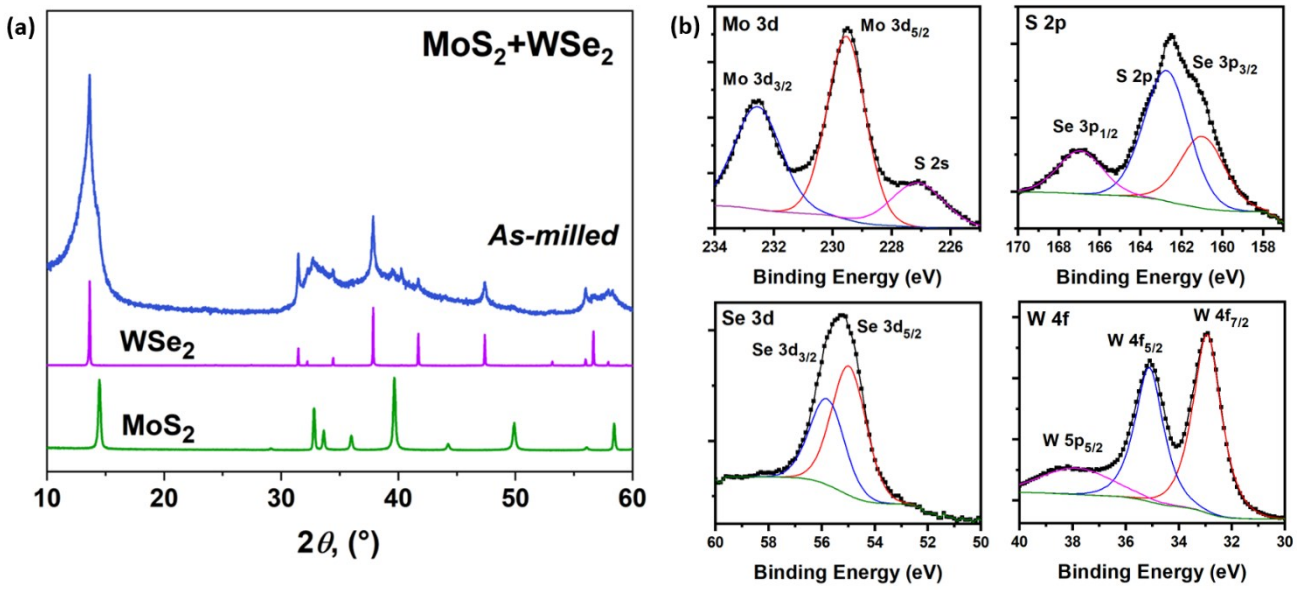

Fig. S3 ($Mo_{0.5}W_{0.5}$)SSe. (a) XRD pattern of *as-milled* equimolar mixtures of MoS_2 and WSe_2. (b) The high-resolution XPS spectra of the fused material showing signals corresponding to Mo 3d, S 2p, Se 3d and W 4f. The XPS spectrum of the annealed ($Mo_{0.5}W_{0.5}$)SSe contains peaks at 229.5 and 232.6 eV corresponding to $Mo^{4+}(3d_{5/2})$ and $Mo^{4+}(3d_{3/2})$ ions and the signal at 227 eV agrees with the position characteristic for S^{2-}(2s) ion.[5] The peaks at 32.9 and 35.1 eV are indicative of $W^{4+}(4f_{7/2}$ and $4f_{5/2})$ in TMDCs[5] while the weak signal at 38 eV suggests the presence of a minor W^{6+} (WO_3) contamination.[5a] Finally, the peak around 162.5 eV corresponds to the unresolved signals by $S^{2-}(2p_{3/2})/S^{2-}(2p_{1/2})$. The additional peaks at ~161 and ~167 eV belong to $Se^{2-}(3p_{3/2})$ and $Se^{2-}(3p_{1/2})$, respectively.[7] The signal at ~55 eV can be assigned to overlapping $3d_{5/2}$ and $3d_{3/2}$ peaks of Se^{2-}.

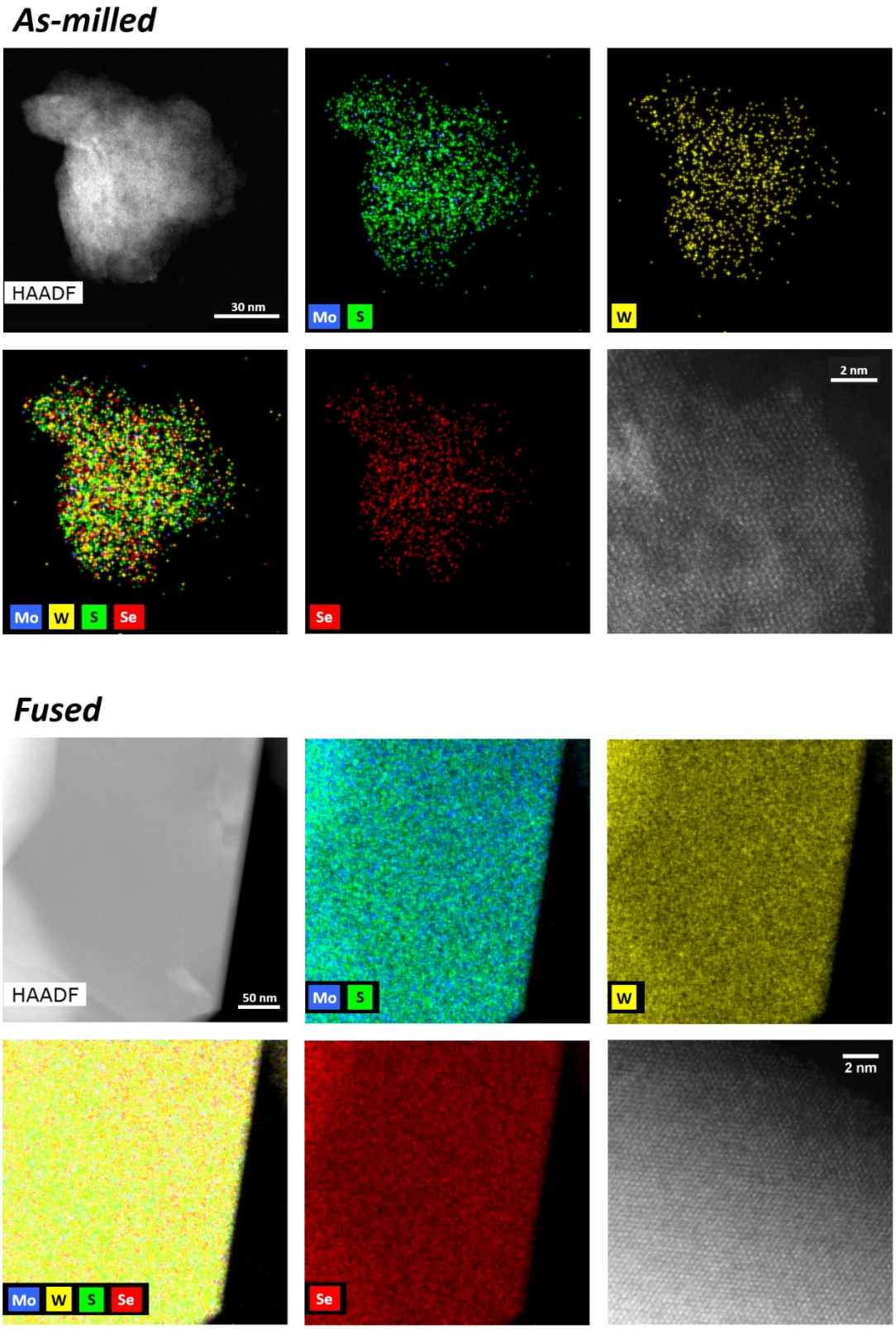

Fig. S4 ($Mo_{0.5}W_{0.5}$)SSe. HAADF-STEM and STEM-EDS images of *as-milled* and fused samples. Intensity variations in the high-resolution HAADF-STEM images are due to different Z-factors of W (brighter spots) and Mo (darker spots). Due to X-ray signal overlap, Mo and S are shown together.

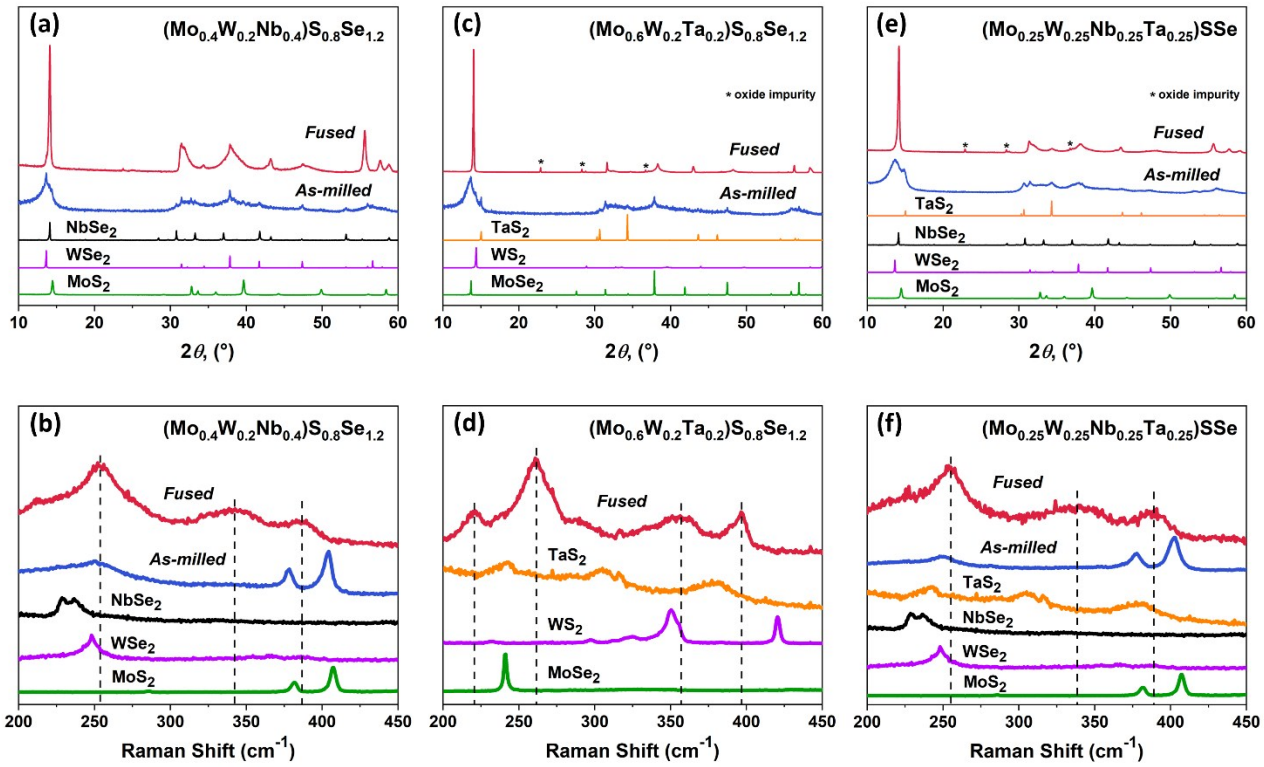

Fig. S5 Five- and six-principal element TMDCs. XRD patterns (a) and Raman spectra (b) of $(Mo_{0.4}W_{0.2}Nb_{0.4})S_{0.8}Se_{1.2}$ and corresponding data for $(Mo_{0.6}W_{0.2}Ta_{0.2})S_{0.8}Se_{1.2}$ (c and d), and $(Mo_{0.25}W_{0.25}Nb_{0.25}Ta_{0.25})SSe$ (e and f). Diffraction patterns and Raman spectra of starting materials are shown as references.

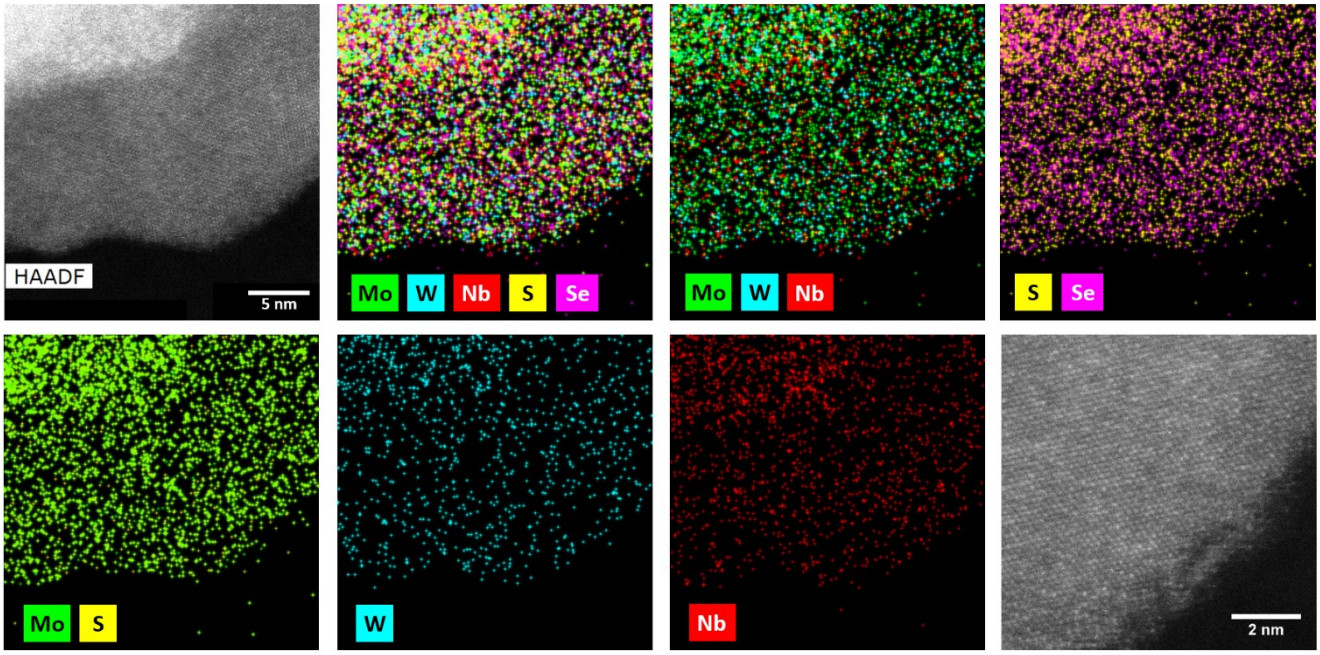

Fig. S6 HAADF-STEM and STEM-EDS images of the fused $(Mo_{0.4}W_{0.2}Nb_{0.4})S_{0.8}Se_{1.2}$. Intensities variation in the high-resolution HAADF-STEM are due to different Z-factors of W (brighter spots), Mo and Nb (darker spots). Due to X-ray signal overlap, Mo and S are shown together.

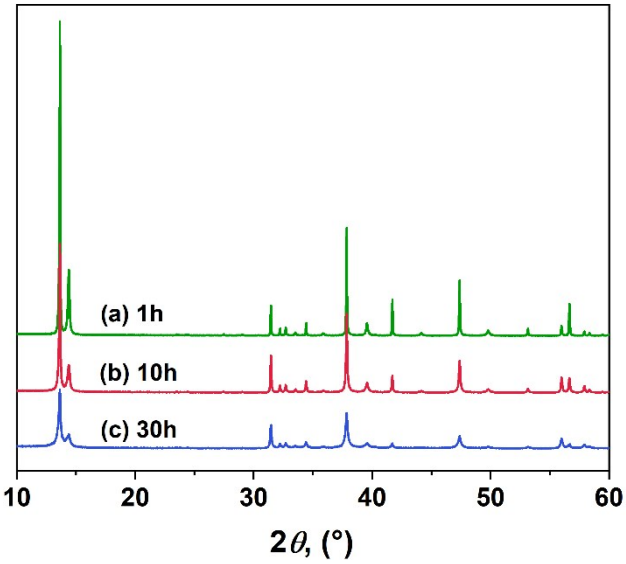

Fig. S7 XRD patterns of the equimolar mixture of MoS_2 and WSe_2 milled in the Fritsch Pulverisette 7 planetary mill at 300 rpm for 1 (a), 10 (b) and 30 hours (c). Starting materials are present in the powder even after 30 hours of processing.

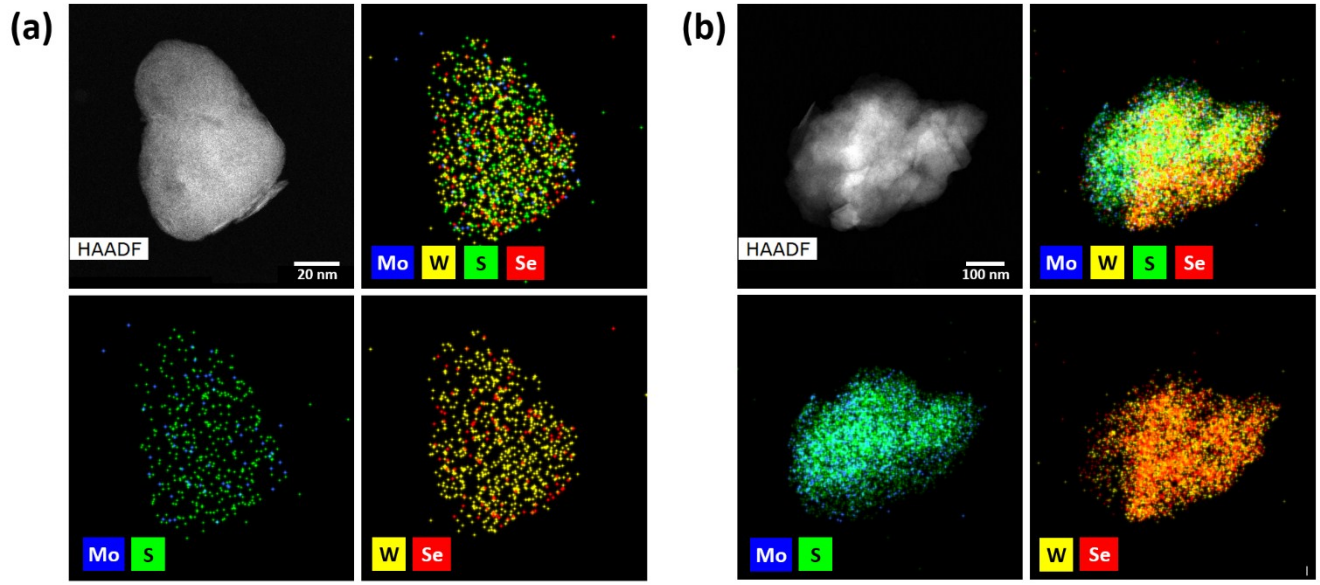

Fig. S8 HAADF-STEM and STEM-EDS images of two types of particles observed in equimolar mixture of MoS_2 and WSe_2 ball-milled at 300 rpm for 30 h.

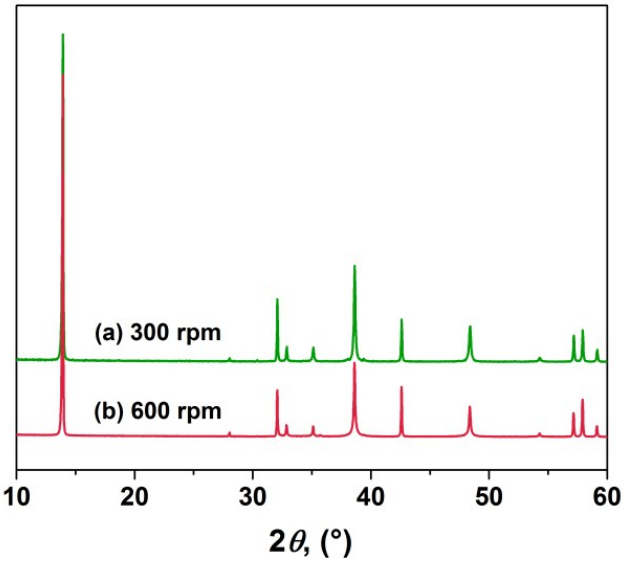

Fig. S9 XRD patterns of the equimolar mixture of MoS_2 and WSe_2 milled in the Fritsch Pulverisette 7 planetary mill for 30 h at 300 rpm (a) and 600 rpm (b) and annealed at 1000 °C for 16 h under helium.

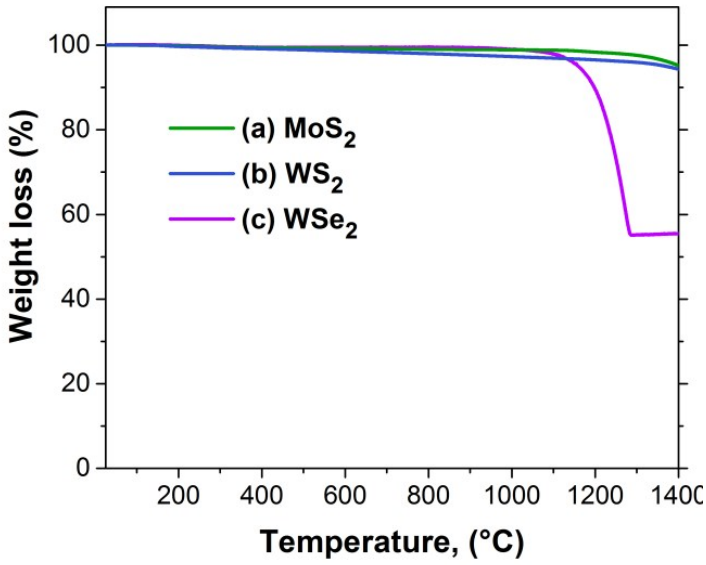

Fig. S10 Thermogravimteric traces of (a) MoS_2, (b) WS_2 and (c) WSe_2.

References

1. (a) L. A. Giannuzzi, J. L. Drown, S. R. Brown, R. B. Irwin and F. A. Stevie, *MRS Proc.*, 1997, **480**, 19–27; (b) T. Yaguchi, T. Kamino, T. Ishitani and R. Urao, *Microsc. Microanal.*, 1999, **5**, 365–370.
2. (*a*) A. S. Gorzalski, C. Donley and O. Coronell, *J. Memb. Sci.* 2017, **522**, 31–44; (*b*) J. J. Friel and C.E. Lyman, *Microsc. Microanal.* 2006, **12**, 2–25.
3. J. R.-C. Roisnel, *Mater. Sci. Forum* **2001**, *378*, 118–123.
4. N. C. Popa, *J. Appl. Crystallogr.* **1998**, *31*, 176–180.
5. (*a*) A. Ambrosi, Z. Sofer and M. Pumera, *Chem. Commun.* 2015, **51**, 8450–8453; (*b*) G. Eda, H. Yamaguchi, D. Voiry, T. Fujita, M. Chen and M. Chhowalla, *Nano Lett.* 2011, **11**, 5111–5116.
6. B. Mahler, V. Hoepfner, K. Liao and G.A. Ozin, *J. Am. Chem. Soc.* 2014, **136**, 14121–14127.
7. R. Naik, S. Jena, R. Ganesan and N. K. Sahoo, *Phys. Status Soldi* 2014, **251**, 661–668.